



www.acsnano.org

Kekulene: On-Surface Synthesis, Orbital Structure, and Aromatic Stabilization

Anja Haags,[®] Alexander Reichmann,[®] Qitang Fan,[®] Larissa Egger, Hans Kirschner, Tim Naumann, Simon Werner, Tobias Vollgraff, Jörg Sundermeyer, Lukas Eschmann, Xiaosheng Yang, Dominik Brandstetter, François C. Bocquet, Georg Koller, Alexander Gottwald, Mathias Richter, Michael G. Ramsey, Michael Rohlfing,* Peter Puschnig,* J. Michael Gottfried,* Serguei Soubatch,* and F. Stefan Tautz



Cite This: ACS Nano 2020, 14, 15766-15775



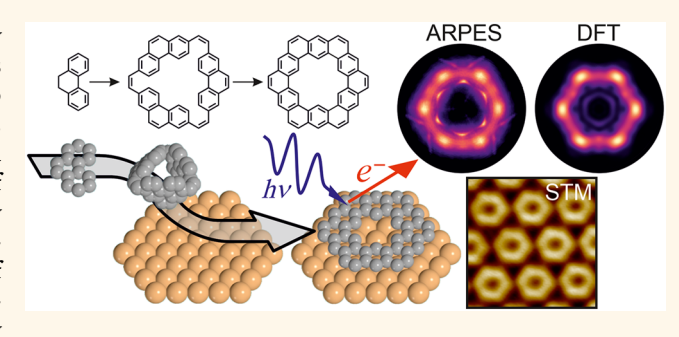
ACCESS

Metrics & More



Supporting Information

ABSTRACT: We revisit the question of kekulene's aromaticity by focusing on the electronic structure of its frontier orbitals as determined by angle-resolved photoemission spectroscopy. To this end, we have developed a specially designed precursor, 1,4,7(2,7)-triphenanthrenacyclononaphane-2,5,8-triene, which allows us to prepare sufficient quantities of kekulene of high purity directly on a Cu(111) surface, as confirmed by scanning tunneling microscopy. Supported by density functional calculations, we determine the orbital structure of kekulene's highest occupied molecular orbital by photoemission tomography. In agreement with a recent aromaticity



assessment of kekulene based solely on C-C bond lengths, we conclude that the π -conjugation of kekulene is better described by the Clar model rather than a superaromatic model. Thus, by exploiting the capabilities of photoemission tomography, we shed light on the question which consequences aromaticity holds for the frontier electronic structure of a π -conjugated molecule

KEYWORDS: kekulene, aromaticity, STM, photoemission, ARPES, DFT

romaticity, a fundamental concept of organic chemistry used to explain the stabilization of cyclic conjugated π -electron systems, has been of special interest to chemists¹ ever since the cyclic structure of benzene has been proposed by Kekulé in 1865.² For kekulene ($C_{48}H_{24}$)—a prototypical cycloarene—a specific aromatic stabilization mechanism has been proposed, namely the π -conjugation in two concentric macrocyclic conjugation paths denoted as [18]annulene and [30]annulene.³-1³ This so-called "superaromaticity" has been debated extensively for many years.⁴-9,12,14-16 In an alternative model, kekulene is thought to consist of six disjoint aromatic sextets, thus fulfilling Clar's rule¹¹ according to which in benzoid molecules the number of disjoint aromatic benzene rings should be maximized and the number of double bonds minimized.

Many attempts to assess kekulene's aromaticity theoretically were solely compared to the first, and until recently the only, experimental study by Staab et al., ^{18–20} who developed a reliable synthesis of kekulene with 80% yield. ¹⁸ The authors analyzed the obtained kekulene microcrystals by mass spectrometry, infrared adsorption and electron spectroscopies,

proton nuclear magnetic resonance (1 H NMR), X-ray diffraction (XRD), and optically detected magnetic resonance (ODMR). 20 However, all of these experiments were hindered by the extremely low solubility of the substance. XRD revealed a substantial variation in bond lengths, and ODMR results indicated a partial compartmentation of the π -system. 19 Based on 1 H NMR results 18 pointing at strong coupling between inner and outer annulene paths and thus suggesting against annulenoid ring currents, Krieger et al. 19 concluded that Clar's sextet model is the better representation of the bonding situation in kekulene.

Recently the synthesis of kekulene has been revisited.^{21,22} Pozo et al.²¹ deposited kekulene on the cold (10 K) Cu(111)

Received: August 13, 2020 Accepted: November 3, 2020 Published: November 13, 2020





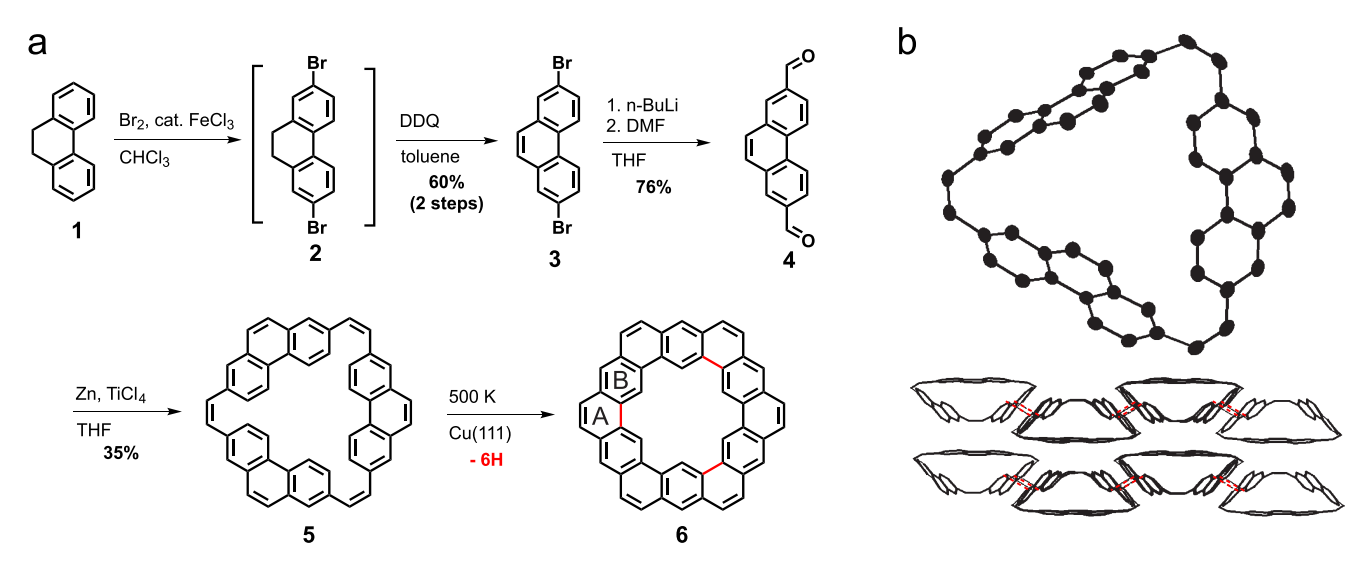


Figure 1. (a) Synthesis of the kekulene precursor 5 by a four-step reaction sequence starting with 9,10-dihydrophenanthrene (1), and the onsurface reaction of 5 leading to kekulene (6). C—C bonds of 6 formed upon cyclodehydrogenation are marked in red. The two nonequivalent benzene rings of 6 are labeled as A and B, respectively. (b) Molecular and lattice structure obtained from single-crystal XRD analysis of 5 (thermal ellipsoids are shown at the 50% probability level and hydrogen atoms are omitted for clarity). The red dashed lines in (b) represent the shortest intermolecular C—C distance (3.34 Å).

surface by rapid thermal evaporation in vacuum. Partial fragmentation due to the high sublimation temperature resulted in an adsorbate consisting of mostly small and often mobile molecules, while only few molecules with the expected hexagonal shape and size of kekulene were observed. Therefore, the investigation of kekulene has only been possible with locally resolved scanning probe methods. Using high-resolution noncontact atomic force microscopy (AFM), Pozo et al. have studied the geometric structure of single adsorbed molecules. By analyzing the contrast in their high-resolution AFM images and comparing with corresponding simulations, they could assess the bond-resolved bond order and hence provide insight into the aromaticity, letting the authors conclude that again the Clar model provides a better description of kekulene.²¹

In contrast to Pozo et al., who focused on structural properties to assess kekulene's aromaticity, in this study, we shed light directly on the electronic structure of kekulene's frontier molecular orbitals by employing angle-resolved photoemission spectroscopy (ARPES). It is important to note that, for such an area-averaging experimental technique, several requirements must be fulfilled: a sufficient number of molecules must be present on the surface, byproducts should be absent, and the majority of these molecules have to be oriented in the same way. To meet these requirements, we developed an on-surface synthesis route enabling the formation of a complete monolayer of well-oriented kekulene molecules, which would not have been possible via vapor deposition of kekulene. Combining density functional theory (DFT) calculations with scanning tunneling microscopy (STM) and photoemission tomography $(PT)^{23,24}$ experiments, we confirm the successful synthesis of a complete ordered kekulene monolayer and investigate the orbital structure of the highest occupied molecular orbital (HOMO). We argue that it can serve as an additional indicator of the type of aromatic bonding and give insight into the aromatic stabilization mechanism of a given molecule. By exploiting the capabilities of photoemission tomography to reveal an orbital-resolved spatial electron

density, ^{23–32} we can unambiguously confirm the Clar model for the aromaticity of kekulene.

RESULTS AND DISCUSSION

Synthesis of Kekulene on Cu(111). The synthesis of the precursor 5 for the dehydrogenative formation of kekulene on Cu(111) proceeds in a four-step reaction sequence as summarized in Figure 1a and described in detail in the Methods section and the Supporting Information (SI). The molecular structure of 5 shown in Figure 1b was proven by X-ray crystallography, which reveals that 5 possesses a nonplanar, highly twisted conformation (cf. SI).

Figure 2a shows an STM image of the as-deposited precursor 5 on a Cu(111) surface. It reveals a number of asymmetric features that are attributed to intact precursor molecules. The bright protrusions in Figure 2a are assumed to represent phenanthrene moieties tilted out of the Cu(111) surface plane due to the nonplanar geometry of 5. Annealing the sample at 500 K drastically changes the structure of the molecular layer. Figure 2b reveals a long-range ordered lattice (domain size up to 100 nm, cf. SI, Figure S1) of planar and aligned hexagonal species. With their central empty pores, they clearly resemble the structure of kekulene. Note that the free molecule belongs to the symmetry group D_{6h}^{19} or, if the small alternating out-of-plane bending of the inner hydrogens is considered, D_{3d} . Therefore, we infer that upon annealing 5 undergoes a cyclodehydrogenation reaction, resulting in a molecular layer of kekulene (6). The density of the molecular layer confirms the high reaction yield of our on-surface synthesis. Note that the formation of large ordered monolayer domains of kekulene on Cu(111) (or indeed any other surface) has not been reported to date.

Density Functional Calculations. We have performed van der Waals corrected density functional calculations for a monolayer of kekulene on Cu(111) by employing a repeated slab approach with six Cu-layers in order to determine the most favorable adsorption structure. As detailed in the SI, we find that the most preferable adsorption configuration is characterized by the hcp hollow site with kekulene's zigzag-

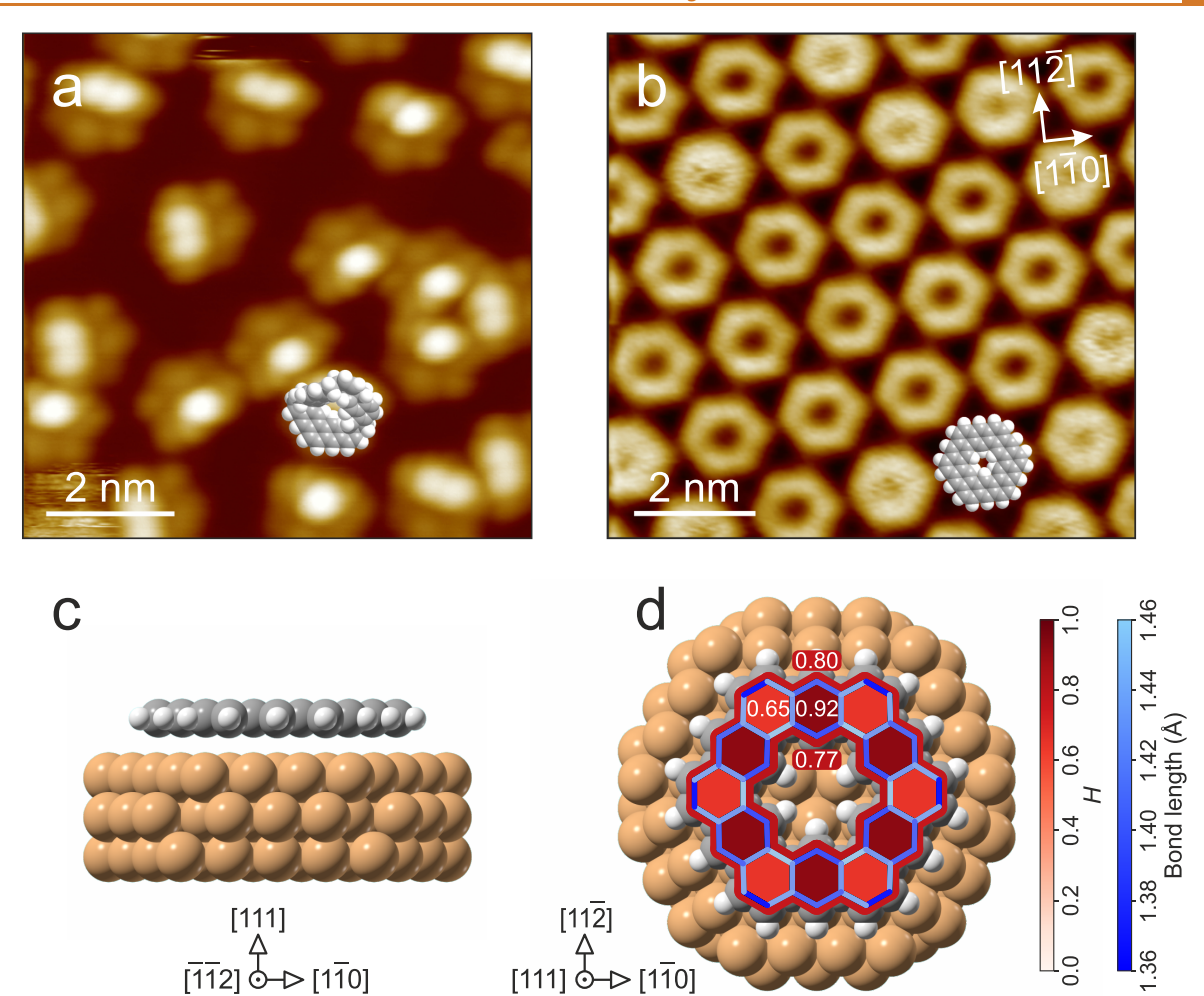


Figure 2. Structural information from STM and DFT. (a and b) STM micrographs of the precursor (5, U = -2.8 V, I = 0.11 nA) and kekulene (6, U = -2.9 V, I = 0.26 nA) on Cu(111), respectively, measured at 100 K. Space-filling molecular models are added to illustrate nonplanar and planar molecular conformations of 5 and 6, respectively. The two different appearances of kekulene in (b) are caused by a slight motion of some molecules, presumably induced by the STM tip. (c and d) Side and top views, respectively, of the relaxed adsorption geometry of kekulene/Cu(111) as obtained by DFT. HOMA values H and the bond lengths of adsorbed kekulene are color coded in red and blue, respectively.

edge oriented along the $[1\overline{1}0]$ direction of Cu(111) (cf. the side and top views depicted in Figure 2c and 2d, respectively). Note that the predicted azimuthal orientation is in agreement with the STM data. The comparably large adsorption height $(\overline{h}_C=3.05~\text{Å})$, a relatively small adsorption energy (123 meV per C atom), and the flat geometry (vertical distortion $\Delta h_C=0.06~\text{Å})$ indicate a rather weak interaction with Cu(111). This agrees with the large mobility of the molecules, reported in ref 21 and confirmed in our own STM experiments (cf. SI, Figure S2).

We have also analyzed the calculated internal geometric structure, i.e., the bond lengths of the relaxed adsorbed kekulene molecule as visualized by the blue color scale in Figure 2d. Moreover, we make use of the harmonic oscillator model of aromaticity (HOMA), which is a commonly applied, purely geometric measure to quantify the aromaticity of molecules. $^{33-36}$ The HOMA value H is defined as

$$H = 1 - \frac{\alpha(n)}{n} \sum_{i=1}^{n} (R_{\text{opt}} - R_i)^2$$
 (1)

H is related to the deformation energy of an aromatic system around its structural optimum, approximated as a harmonic

potential around an optimum C–C bonding distance $R_{\rm opt}$. $R_{\rm opt}$ itself follows from the minimization of the deformation energy and represents an ideal aromatic system. The original and fundamental idea is that each pair of carbon atoms can be involved in both a σ - and a π -bond, with $R_{\sigma} > R_{\pi}$. The actual bonding distance R_i represents a compression of R_σ and an extension of R_{π} . Both terms cost energy. While this energy penalty is minimized at R_{opt} in any given molecule the R_i may deviate from Ropt which is interpreted as a local dearomatization of the molecule. The HOMA value is a sum over ndearomatizing contributions in the relevant part of the molecule. Note that H = 1 signals perfect aromaticity, while smaller H values correspond to weaker aromatic stabilization. In our calculations, the normalization parameter $\alpha(n)$ is taken from ref 37 and Ropt is calculated as the average of single- and double-bond lengths of trans-1,3-butadiene as obtained by our DFT calculations, yielding $R_{\text{opt}} = 1.403 \text{ Å (cf. SI for details)}$.

We use the HOMA (red color scale and white numbers in Figure 2d) here as a reference for our orbital-based analysis of aromaticity to be introduced later. While the HOMA is not the only yardstick of aromaticity, 11 other suggested criteria of aromaticity based on geometric, energetic, magnetic, and

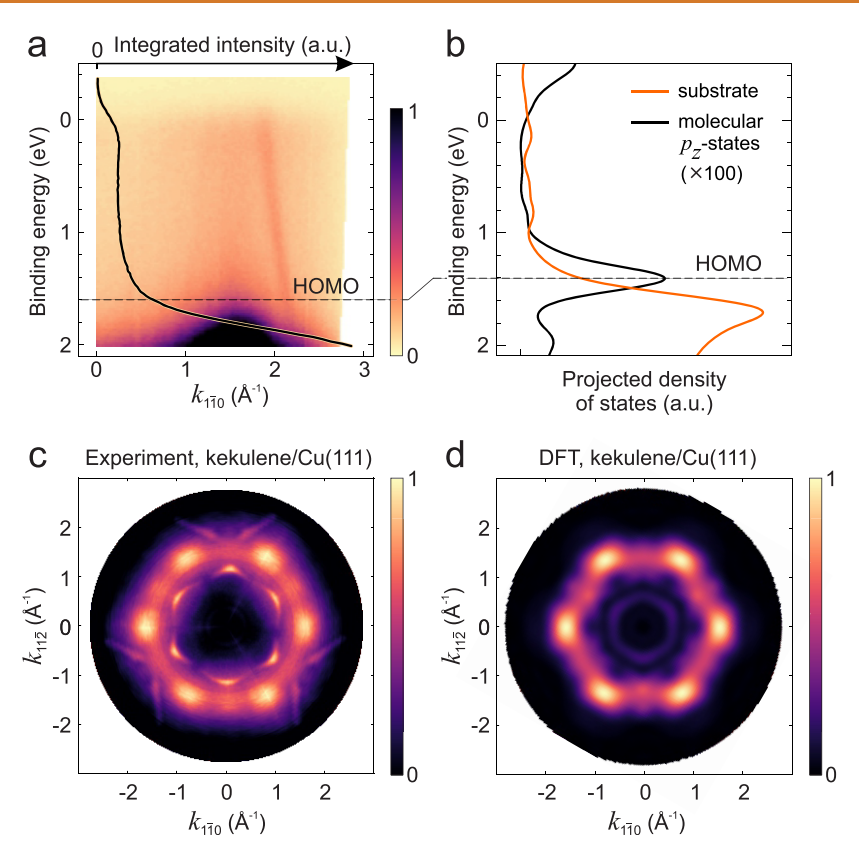


Figure 3. Angle-resolved photoemission data of kekulene/Cu(111) from experiment and theory. (a) ARPES band map along the $[1\overline{1}0]$ direction in an energy range of about 2 eV below the Fermi edge. The black line shows an angle-integrated energy distribution curve. (b) Density of states projected onto substrate (orange) and molecular p_z states (black) from DFT. (c and d) Experimental and simulated momentum maps at the respective binding energies of the HOMO as indicated by the dashed lines in (a) and (b). Photoemission was excited by p-polarized light of 35 eV photon energy.

electronic properties of molecules are found to be in good correlation with the HOMA. 11,38,39 As an advantage of the HOMA concept, the partial equalization of bond lengths in aromatic systems, which is quantified by the HOMA value, can be easily obtained from DFT calculations. In addition, not only the aromaticity of the molecule as a whole but also the aromaticity of any cyclic conjugation path can be quantified, allowing, e.g., the separate description of local, peripheral and global aromaticities. Here, we evaluate H for four conjugation paths of the surface-adsorbed kekulene molecule, namely for the two inequivalent sextets A (ring A in Figure 1a, $H_{\rm A}=0.65$) and B (ring B in Figure 1a, $H_{\rm B}=0.92$) as well as the [18]annulene and [30]annulene paths, respectively 40,41 ($H_{\rm [18]}=0.77$ and $H_{\rm [30]}=0.80$), each of which fulfills Hückel's 4n+2 condition of aromaticity and is therefore a possible candidate for affecting the aromatic stabilization of kekulene.

On the one hand, the HOMA values displayed in Figure 2d seem to indicate a propensity of kekulene toward Clar's limit as already noted by others, $^{3,5,11,19,21}_{,,19,21}$ because we observe that ring B exhibits the largest HOMA value ($H_{\rm B}=0.92$). On the other hand, this conclusion is not unambiguous, because with $H_{[30]}=0.80$, the [30]annulene path appears strongly aromatic as well. Also, the HOMA quite obviously exaggerates the peripheral aromaticity of kekulene, leading to the counterintuitive result that the aromaticity of the larger [30]annulene path is predicted to be larger than the one of the smaller [18]annulene path, in contradiction to the Hückel rule, according to which π -systems with 4n+2 electrons are more stable for smaller n. Note, however, that such arguments,

based on the Hückel molecular orbital method, might be oversimplified and neglect, for instance, the coupling between the two annulenes in kekulene. An overestimation of peripheral aromaticities is a well-known problem of the HOMA concept, 11 and it should be noted that there exist more sophisticated approaches to access the aromaticity of annulenes. 12 To conclude, from the purely structural deliberations, the relative importance of both postulated types of aromaticity in kekulene, Clar versus superaromatic model, cannot be inferred. Nevertheless, it is fair to state that the above findings regarding the HOMA assess the intrinsic aromaticity of kekulene, and in particular that the influence of the surface on the aromaticity of the adsorbed molecule is moderate (cf. SI, Table S4).

Photoemission Tomography. Up to this point, we solely concentrated on the analysis of aromaticity via bond lengths. However, aromaticity is an electronic stabilization of the molecule. To assess electronic properties of kekulene, we consult PT that can provide a complementary measure for aromaticity as we will show now.

In the experiment, a photoemission from a molecular state appears at the binding energy of 1.6 eV indicated by the dashed line in Figure 3a, i.e., only slightly above the onset of the Cu d-band, and is hence barely resolved in the energy distribution curve and band map. The computed projected density of states (pDOS) for kekulene/Cu(111) (Figure 3b) suggests that this emission can be assigned to the HOMO of kekulene, which, in the gas phase, belongs to the e_{1g} irreducible representation and is composed of a doubly degenerate state.

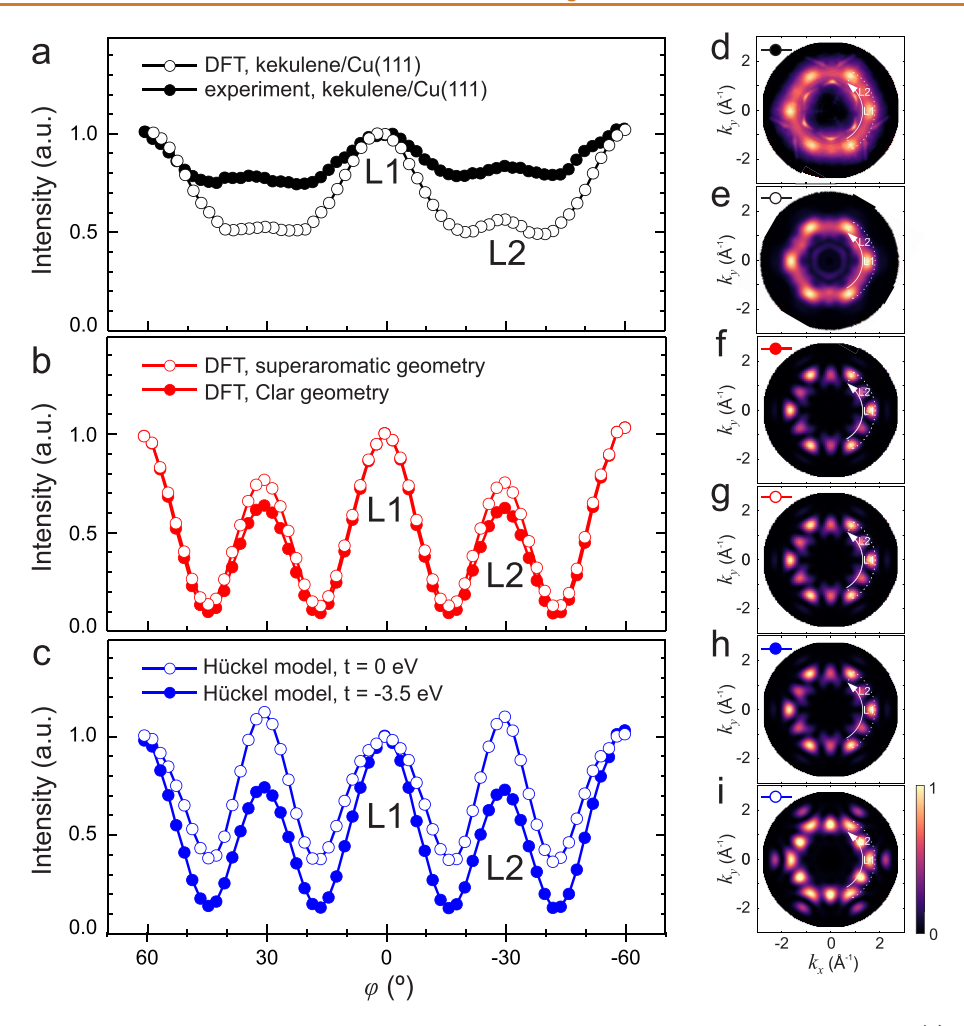


Figure 4. Comparison of experimental and simulated azimuthal ARPES intensity profiles of the kekulene HOMO. (a) Azimuthal profiles of the experiment (full symbols) and the DFT calculation of kekulene/Cu(111) (open symbols), extracted from the momentum maps shown in panels (d) and (e), respectively. (b) Simulated profiles from DFT gas-phase calculations of kekulene in the Clar geometry (full symbols) and superaromatic geometry (open symbols). The corresponding maps are shown in panels (f) and (g). (c) Simulated profiles from a Hückel model in which the coupling between inner and outer annulenes is set to t = -3.5 eV (full symbols) and to t = 0 (open symbols). The corresponding maps are shown in panels (h) and (i). Nonequivalent intensity lobes are labeled as L1 and L2. White lines in the momentum maps show the area used for intensity integration.

To confirm this assignment, we measure a momentum map of the photoemission intensity distribution at the respective constant binding energy. Figure 3c shows clear signatures of the molecule, namely six major lobes at $k_{\parallel} \approx 1.6 \ {\rm \AA}^{-1}$ and six interjacent minor lobes at a slightly smaller $k_{\parallel} \approx 1.5 \text{ Å}^{-1}$. In addition, the sharper features signal emissions from the copper sp-bands. The experimental momentum map is in excellent agreement with the simulated momentum map for the kekulene/Cu(111) HOMO at 1.4 eV depicted in Figure 3d. A number of conclusions can be drawn from this agreement: First, it unambiguously confirms the successful on-surface synthesis of kekulene on Cu(111) resulting in large (up to 100 nm, cf. SI, Figute S1) well-orientated domains. Second, the azimuthal alignment of the molecule, as already inferred from STM and DFT, is also confirmed by the photoemission data in which the sharp sp-band features indicate the substrate's orientation.

We now address the primary goal of our paper to demonstrate that PT, since it is directly related to the orbital structure of frontier molecular orbitals, provides substantial insights regarding the aromaticity of molecules. To this end, Figure 4 shows the experimental and various simulated

HOMO momentum maps, and in particular, it compares azimuthal intensity profiles passing through the major (L1) and minor (L2) lobes of the HOMO momentum map. Panel (a) depicts the experimental intensity profile (filled symbols) and the corresponding simulation result for kekulene/Cu(111) (open symbols) extracted from the momentum maps already presented in Figure 3c and 3d, respectively, which are replicated here for convenience in Figure 4d and 4e. These intensity profiles confirm the qualitative agreement between theory and experiment. The barely comparable backgrounds of experimental and theoretical data for the states in the vicinity of the Cu d- and sp-bands prevent a full quantitative comparison of the intensity ratio between major and minor lobes

In order to investigate how modifications in the geometry and/or electronic structure of kekulene are reflected in momentum maps of the HOMO emission, we next simulate momentum maps for the two idealized and extreme cases of the Clar and the superaromatic models of free kekulene, respectively. For the Clar model, we set $R_{\rm sextet} = R_{\rm opt}$ thus requiring maximal aromaticity of these sextets ($H_{\rm B}=1$). In contrast, for the superaromatic model we stipulate that all

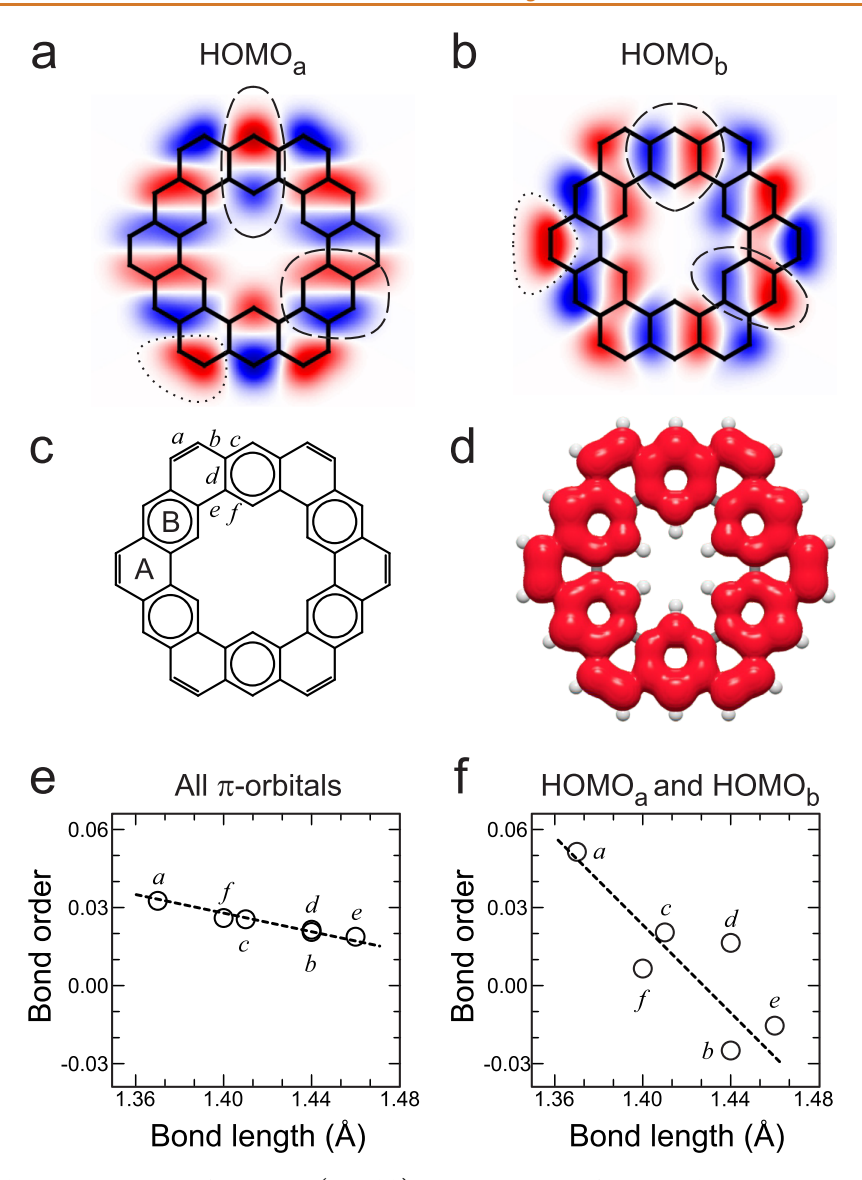


Figure 5. The frontier electronic structure of kekulene. (a and b) Nodal structure of the two degenerate orbitals comprising the HOMO, denoted HOMO_a and HOMO_b, respectively, calculated with the Hückel model. (c) Chemical structure drawing of kekulene in the Clar model with six inequivalent C–C bonds labeled as a to f. (d) Charge density distribution of the HOMO (Hückel model). (e and f) Correlation between the C–C bond lengths of gas-phase kekulene as determined from DFT and a normalized bond order parameter from Hückel theory taking into account either all 24 occupied π -orbitals or only the degenerate HOMO (m = 23 to 24) orbital. Details are given in the text.

bonds in the annulene paths are identical, with $R_{[18]} = R_{[30]} =$ $R_{\text{opt}} = 1.403 \text{ Å to constrain that } H_{[18]} = H_{[30]} = 1. \text{ Using these}$ fixed geometries and neglecting the presence of the substrate, we employ DFT (cf. SI for details) to compute the orbital structure of the HOMO and the corresponding momentum maps for these two model geometries of free kekulene. Figure 4b displays the intensity profiles of these idealized Clar (full symbols) and superaromatic (open symbols) geometries, respectively. As is evident also from the corresponding momentum maps shown in Figure 4f and 4g, respectively, the overall symmetry and appearance of the momentum maps in Figure 4d and 4e as well as the fact that in Figure 4a the intensity of lobe L1 is considerably larger than that of lobe L2 are preserved in both model calculations. On the one hand, this can be taken as another indication that the interaction of kekulene with Cu(111) is rather weak and therefore neglecting the substrate completely when discussing the electronic

structure of kekulene seems a reasonable approach (Yet, some discrepancies between the results of DFT simulations for the adsorbed and free kekulene exist, e.g., the background intensity in Figure 4a and b, and can be attributed to the effect of the substrate, namely a broadening of the molecular states due to the coupling to the metal states as well as additional emission from the substrate.) On the other hand, and more importantly, when changing from the Clar to the superaromatic geometry, we notice only moderate changes in the orbital structure of the HOMO observed as an ∼10% increase in the intensity of the minor lobe L2. It is important to note that this finding is insensitive to the choice for the exchangecorrelation functional, even when incorporating a substantial fraction of Hartree-Fock exchange (cf. SI, Figure S3). Thus, from our DFT calculations it becomes evident that changing the geometry of the molecular backbone (bond lengths) from Clar-type to superaromatic does not affect the electronic system of kekulene profoundly. Generally speaking, this means that small variations in the geometric structure of the molecule, i.e., a system with an energy gap, does not change the nodal structure of the wave function. This noteworthy fact is illustrated in Figure S7 (cf. SI), where we compare the orbital structure of the kekulene's HOMO and HOMO—1 as obtained for the Clar and the superaromatic geometry.

Therefore, in order to impose the superaromatic stabilization by the annulene conjugation paths, we approximate the π -electron system of kekulene with a simple Hückel model.⁴³ This approach provides a way to tune the coupling between the inner [18] annulene path and the outer [30] annulene path by adjusting the hopping parameter t for corresponding bonds connecting them (see SI for details). In particular, a value of t = -3.5 eV leads to approximately the DFT result for free kekulene, as evidenced by the HOMO momentum map depicted in Figure 4h and the corresponding azimuthal intensity profile shown in Figure 4c (full symbols). If the coupling between the annulenes is completely suppressed (t = 0), the doubly degenerate HOMO is now concentrated exclusively around the outer [30] annulene path (cf. SI, Figure S7d,h) and could indeed be termed "superaromatic" from an electronic structure point of view. As can be seen from Figure 4i (cf. also SI, Figure S7l), the corresponding momentum map is also markedly different. The formerly minor lobe L2 is almost doubled in intensity and becomes the brightest feature. Also, there are six additional lobes at larger $k_{\parallel} \approx 2.1~{\rm \AA}^{-1}$ which are a result of the confinement of the electrons to only the outer annulene path, leading to a larger spread in momentum space. None of these signatures are observed in the experimental momentum map of the HOMO (compare Figure 4d or 3c). Thus, we conclude that photoemission tomography indeed excludes a superaromatic state. Instead, all PT evidence points toward the Clar model also from an electronic structure perspective.

CONCLUSIONS

It remains to be clarified how exactly the orbital structure of the HOMO alone, as accessible via photoemission tomography, may serve as a sufficient measure for the aromaticity of kekulene, apparently not requiring the consideration of all π -electrons, i.e., including those in deeper-lying orbitals. To approach this question, we employ the Hückel model with t = -3.5 eV and analyze the orbital structures of the doubly degenerate HOMO of kekulene, denoted as HOMO_a and HOMO_b (Figure 5a and 5b). We observe that the electrons in the HOMO are confined to neither the inner nor the outer annulene path. Instead, the frontier electrons are delocalized over both annulene paths, and the pattern of this delocalization is already a portent of the Clar model, as a straightforward visual inspection of the electron distribution in HOMO_a and HOMO_b in Figure 5a and 5b shows: locally, the pair of kekulene HOMOs consists of benzene-like HOMOs (marked by the dashed lines in Figure 5a and 5b) which are located at exactly those carbon rings (ring B) where the Clar model predicts aromatic sextets (Figure 5c), while a pronounced double bond lobe appears at the corners of kekulene (marked by dotted lines in Figure 5a and 5b). The Clar structure also becomes clearly apparent when computing the charge density as a sum of HOMO_a and HOMO_b electron distributions (Figure 5d) and comparing it with a chemical structure drawing of the Clar model of kekulene (Figure 5c): the six disjoint aromatic sextets

characteristic for the Clar model can be recognized in the charge distribution of the HOMO, as well as the isolated double bonds at the corners. The evolution of kekulene's HOMO from the doubly degenerate HOMO and HOMO-1 of concentric but initially electronically decoupled [18]-annulene and [30]annulene as the coupling is turned on, shown as a video in the SI, reveals that its Clar-like structure is in fact an immediate consequence of the interannulene coupling in kekulene and its effect on the frontier orbitals.

The significance of the HOMO for the aromaticity of kekulene is confirmed by considering its contribution to the bond order. In general, the bond order relates orbital structure to the bond lengths in a π -conjugated molecule, and thus also to structure-derived aromaticity parameters such as the HOMA values. We define a bond order parameter b_{ij} , which we normalize by the number of contributing π -electrons N, for a given bond between carbon atoms labeled i and j in the following way:

$$b_{ij} = \frac{2}{N} \sum_{m=1}^{N} a_i(m) \ a_j(m)$$
 (2)

Here, $a_i(m)$ is the contribution of the p_z orbital at carbon atom i to the molecular orbital m, as resulting from the solution of the Hückel model. If all 24 occupied π -orbitals of kekulene are included in the summation of eq 2, i.e., m = 1 to 24, plotting the bond order parameter against the DFT-optimized bond lengths for kekulene yields a clear and almost linear correlation (Figure 5e). This indicates that through the bond order parameter the nodal patterns of all occupied orbitals together determine the final bond lengths and thus also the HOMAderived aromaticity in kekulene. For example, all occupied π -orbitals together lead to a large bond order for bond a (cf. Figure 5c,e), which therefore is short (DFT-calculated value of $d_a = 1.37 \text{ Å}$) and can be interpreted as having a strong double bond character, while bond e with its smaller bond order is longer (DFT-calculated value of $d_e = 1.46 \text{ Å}$) and thus appears to be more of single bond character. However, there is also a pronounced correlation if we only include the doubly degenerate $HOMO_a$ and $HOMO_b$ in the summation (m =23 to 24, Figure 5f). This reveals that the correct bond order pattern is already present in the occupied frontier orbital. It is therefore not surprising that the nodal patterns of the HOMO, which we measure in PT, are indicative of kekulene's aromaticity. Indeed, the shortest C-C bond (bond a) has a strong contribution of the HOMO charge density, while the longest C-C bond (bond e) does not (cf. Figure 5d). The disproportionate effect of the uppermost occupied π -orbitals to produce the final linear trend observed in Figure 5e also becomes apparent if only the lower half of the occupied π -states (m = 1 to 12) is included in the summation of eq 2, because then the trend is completely reversed (cf. SI, Figure S8a). Interestingly, if the interannulene coupling is switched off (t = 0), then the resulting bond order suggests all bonds to be of equal lengths, which is indeed the case if one was to optimize the structure of individual [18] annulene or individual [30] annulene paths.

In summary, we present an efficient on-surface synthesis route with a high reaction yield resulting in a well-oriented monolayer of kekulene on Cu(111). This allows us to apply the photoemission tomography technique to directly address the symmetry and spatial structure of the charge distribution of the frontier kekulene electronic level, its degenerate HOMO.

By comparing the experimental momentum map of the HOMO with photoemission simulations for kekulene in various geometric and electronic states, we analyze the aromaticity of kekulene. We find that imposing either the Clar- or the superaromatic-type geometry influences the nodal structure of the two degenerate HOMO components only very slightly and, accordingly, leaves the simulated photoemission maps mainly unaffected. Only when suppressing the coupling of the π -electron system between two annulene paths, as we demonstrate within the Hückel molecular orbital model, a true superaromatic state characterized by a spatial confinement of the HOMO electron density to the outer annulene, accompanied by a pronounced change in the photoemission momentum map, can be mimicked (cf. SI, Figure S7). This comparison between measured and simulated momentum maps rules out a superaromatic state in kekulene but rather favors a Clar-type structure. Our work demonstrates that the spatial structure of occupied frontier orbitals can indeed be taken as a valid yardstick for the aromaticity of π -conjugated molecules and that photoemission tomography is a powerful complementary method to assess the role of aromatic stabilization in π -conjugated molecules.

METHODS AND EXPERIMENTAL DETAILS

The synthesis of the precursor **5** starts with commercially available 9,10-dihydrophenanthrene (1), which was regioselectively brominated to form 2,7-dibromo-9,10-dihydrophenanthrene (2) by applying a procedure of Wang et al. 45 using bromine in the absence of light. Compound **2** was oxidatively aromatized to the corresponding 2,7-dibromophen-anthrene (3). Subsequently, the latter was converted into bis-aldehyde (4) via Br–Li exchange at low temperature using *n*-butyl lithium and trapping the lithiated intermediate with dimethylformamide (DMF) and aqueous workup. Aldehyde **4** was coupled in the last step to kekulene precursor **5** using a McMurry reaction protocol established for related targets by Majewski et al. 22 This protocol requires dropwise addition of **4** to a diluted reaction solution of low-valent titanium reagent formed *in situ* from titanium tetrachloride and zinc.

The kekulene precursor 5 could be obtained as a beige crystalline solid in 35% yield next to higher oligomers of 4 via purification by column chromatography followed by recrystallization. The molecular structure and conformation of 5 were proven by X-ray crystallography (Figure 1b). X-ray diffractive single crystals of 5 were obtained by slow diffusion of *n*-pentane into a saturated solution of 5 in chloroform. Details of chemical synthesis and characterization of 5 are provided in the SI.

The preparation of kekulene/Cu(111), photoemission, and STM experiments were performed in an ultrahigh vacuum system with a base pressure in the 10^{-10} mbar range. Samples of Cu(111) were cleaned by repeating cycles of sputtering by $\mathrm{Ar^+}$ ions (1.0 kV) and annealing (850 K). The molecular precursor 5 was deposited from a Knudsen-type effusion cell at 550 K onto the Cu(111) surface kept at room temperature. To trigger the reaction of cyclodehydrogenation resulting in kekulene, submonolayer films of 5 on Cu(111) were annealed at 500 K.

STM was performed with an STM Aarhus 150 microscope from SPECS GmbH. During measurements the samples were kept at 100 K.

ARPES and PT were conducted at the Metrology Light Source insertion device⁴⁶ beamline of the Physikalisch-Technische Bundesanstalt (PTB, Germany). *p*-Polarized ultraviolet light (35 eV photon energy) was used with the angle of incidence of 40°. Photoelectrons were collected with the toroidal electron spectrometer.⁴⁷ For the experimental spectrum, band map, and momentum map shown in Figure 3, the photoemission intensity in the emission angle range from 0° (sample normal) to +85° was used. Momentum maps were recorded by rotating the sample in the azimuthal direction

in 2° steps and measuring the photoemission intensity at a constant kinetic energy of the electrons. This results in the full photoelectron distribution in the (k_x, k_y) plane perpendicular to the sample normal. Details about the DFT calculations and the photoemission tomography simulations are given in the SI.

ASSOCIATED CONTENT

5 Supporting Information

The Supporting Information is available free of charge at https://pubs.acs.org/doi/10.1021/acsnano.0c06798.

Experimental details, details of chemical synthesis, kekulene/Cu(111) sample preparation, STM, ARPES and PT, details of computational analysis. (PDF) video demonstrating the effect of electronic coupling between inner and outer annulene paths on the HOMO and HOMO–1 states of free kekulene (MP4) SWP148.pdf and swp148loesen.cif: CIF check and CIF files for kekulene precursor 1,4,7(2,7)-triphenanthrenacyclononaphane-2,5,8-triene. (CIF)

AUTHOR INFORMATION

Corresponding Authors

Michael Rohlfing — Institut für Festkörpertheorie, Westfälische Wilhelms-Universität Münster, 48149 Münster, Germany; Email: michael.rohlfing@uni-muenster.de

Peter Puschnig — Institut für Physik, Karl-Franzens-Universität Graz, NAWI Graz, 8010 Graz, Austria; orcid.org/0000-0002-8057-7795;

Email: peter.puschnig@uni-graz.at

J. Michael Gottfried – Fachbereich Chemie, Philipps-Universität Marburg, 35032 Marburg, Germany; o orcid.org/0000-0001-5579-2568;

Email: michael.gottfried@chemie.uni-marburg.de

Serguei Soubatch — Peter Grünberg Institut (PGI-3), Forschungszentrum Jülich, 52425 Jülich, Germany; Jülich Aachen Research Alliance (JARA), Fundamentals of Future Information Technology, 52425 Jülich, Germany; orcid.org/0000-0002-1455-0260; Email: s.subach@fzjuelich.de

Authors

Anja Haags – Peter Grünberg Institut (PGI-3), Forschungszentrum Jülich, 52425 Jülich, Germany; Jülich Aachen Research Alliance (JARA), Fundamentals of Future Information Technology, 52425 Jülich, Germany; Experimentalphysik IV A, RWTH Aachen University, 52074 Aachen, Germany

Alexander Reichmann – Institut für Physik, Karl-Franzens-Universität Graz, NAWI Graz, 8010 Graz, Austria

Qitang Fan – Fachbereich Chemie, Philipps-Universität Marburg, 35032 Marburg, Germany

Larissa Egger – Institut für Physik, Karl-Franzens-Universität Graz, NAWI Graz, 8010 Graz, Austria

Hans Kirschner – Physikalisch-Technische Bundesanstalt (PTB), 10587 Berlin, Germany

Tim Naumann – Fachbereich Chemie, Philipps-Universität Marburg, 35032 Marburg, Germany

Simon Werner – Fachbereich Chemie, Philipps-Universität Marburg, 35032 Marburg, Germany

Tobias Vollgraff – Fachbereich Chemie, Philipps-Universität Marburg, 35032 Marburg, Germany

Jörg Sundermeyer – Fachbereich Chemie, Philipps-Universität Marburg, 35032 Marburg, Germany

- Lukas Eschmann Institut für Festkörpertheorie, Westfälische Wilhelms-Universität Münster, 48149 Münster, Germany
- Xiaosheng Yang Peter Grünberg Institut (PGI-3), Forschungszentrum Jülich, 52425 Jülich, Germany; Jülich Aachen Research Alliance (JARA), Fundamentals of Future Information Technology, 52425 Jülich, Germany; Experimentalphysik IV A, RWTH Aachen University, 52074 Aachen, Germany; orcid.org/0000-0002-7632-0401
- Dominik Brandstetter Institut für Physik, Karl-Franzens-Universität Graz, NAWI Graz, 8010 Graz, Austria
- François C. Bocquet Peter Grünberg Institut (PGI-3), Forschungszentrum Jülich, 52425 Jülich, Germany; Jülich Aachen Research Alliance (JARA), Fundamentals of Future Information Technology, 52425 Jülich, Germany
- Georg Koller Institut für Physik, Karl-Franzens-Universität Graz, NAWI Graz, 8010 Graz, Austria; ⊙ orcid.org/0000-0001-7741-2394
- Alexander Gottwald Physikalisch-Technische Bundesanstalt (PTB), 10587 Berlin, Germany
- **Mathias Richter** Physikalisch-Technische Bundesanstalt (PTB), 10587 Berlin, Germany
- Michael G. Ramsey Institut für Physik, Karl-Franzens-Universität Graz, NAWI Graz, 8010 Graz, Austria
- F. Stefan Tautz Peter Grünberg Institut (PGI-3), Forschungszentrum Jülich, 52425 Jülich, Germany; Jülich Aachen Research Alliance (JARA), Fundamentals of Future Information Technology, 52425 Jülich, Germany; Experimentalphysik IV A, RWTH Aachen University, 52074 Aachen, Germany

Complete contact information is available at: https://pubs.acs.org/10.1021/acsnano.0c06798

Author Contributions

[@]A.H., A.R., and Q.F. contributed equally to this work.

Notes

The authors declare no competing financial interest. The preprint version is available online.⁴⁸ Raw data are available at the Jülich DATA public repository.⁴⁹

ACKNOWLEDGMENTS

Financial support from the Deutsche Forschungsgemeinschaft (DFG) (Projects Po 2226/2-1, Ri 804/8-1, Go 1812/2-1, 223848855-SFB 1083 "Structure and Dynamics of Internal Interfaces") and the Austrian Science Fund (FWF) (Projects P27649-N20, P27427-N20, and I3731) is gratefully acknowledged. The computational results have been achieved using the computing facilities of the University of Graz and the Vienna Scientific Cluster (VSC3), as well as those of the John von Neumann Institute for Computing (NIC) on the GCS Supercomputer JUWELS at Jülich Supercomputing Centre (JSC). We thank Hendrik Kaser (PTB, Berlin) and John Riley (La Trobe University, Australia) for experimental support.

REFERENCES

- (1) Balaban, A. T. Is Aromaticity Outmoded? Pure Appl. Chem. 1980, 52, 1409-1429.
- (2) Kekulé, M. A. Sur la Constitution des Substances Aromatique. Bulletin mensuel de la Société chimique de Paris 1865, 3, 98.
- (3) Aihara, J.-i. On the Number of Aromatic Sextets in a Benzenoid Hydrocarbon. *Bull. Chem. Soc. Jpn.* **1976**, *49*, 1429–1430.
- (4) Cioslowski, J.; Mixon, S. T.; Edwards, W. D. Weak Bonds in the Topological Theory of Atoms in Molecules. *J. Am. Chem. Soc.* **1991**, 113, 1083–1085.

- (5) Aihara, J.-i. Is Superaromaticity a Fact or an Artifact? The Kekulene Problem. J. Am. Chem. Soc. 1992, 114, 865–868.
- (6) Jiao, H.; von Ragué Schleyer, P. Is Kekulene Really Superaromatic? *Angew. Chem., Int. Ed. Engl.* **1996**, 35, 2383–2386.
- (7) Zhou, Z. Are Kekulene, Coronene, and Corannulene Tetraanion Superaromatic? Theoretical Examination Using Hardness Indices. *J. Phys. Org. Chem.* **1995**, *8*, 103–107.
- (8) Aihara, J.-i.; Makino, M.; Ishida, T.; Dias, J. R. Analytical Study of Superaromaticity in Cycloarenes and Related Coronoid Hydrocarbons. *J. Phys. Chem. A* **2013**, *117*, 4688–4697.
- (9) Aihara, J.-i. A Simple Method for Estimating the Superaromatic Stabilization Energy of a Super-Ring Molecule. *J. Phys. Chem. A* **2008**, 112. 4382–4385.
- (10) Buttrick, J. C.; King, B. T. Kekulenes, Cycloarenes, and Heterocycloarenes: Addressing Electronic Structure and Aromaticity through Experiments and Calculations. *Chem. Soc. Rev.* **2017**, *46*, 7–20.
- (11) Setiawan, D.; Kraka, E.; Cremer, D. Quantitative Assessment of Aromaticity and Antiaromaticity Utilizing Vibrational Spectroscopy. *J. Org. Chem.* **2016**, *81*, 9669–9686.
- (12) Lahti, P. M. Localization of Aromaticity in Fused-Ring Cycloarene Systems. Prediction by an Effective Molecular Mechanics Model. *J. Org. Chem.* **1988**, *53*, 4590–4593.
- (13) Allinger, N. L.; Li, F.; Yan, L.; Tai, J. C. Molecular Mechanics (MM3) Calculations on Conjugated Hydrocarbons. *J. Comput. Chem.* **1990**, *11*, 868–895.
- (14) Liu, C.; Ni, Y.; Lu, X.; Li, G.; Wu, J. Global Aromaticity in Macrocyclic Polyradicaloids: Hückel's Rule or Baird's Rule? *Acc. Chem. Res.* **2019**, *52*, 2309–2321.
- (15) Chen, Z.; King, R. B. Spherical Aromaticity: Recent Work on Fullerenes, Polyhedral Boranes, and Related Structures. *Chem. Rev.* **2005**, *105*, 3613–3642.
- (16) Miyoshi, H.; Nobusue, S.; Shimizu, A.; Tobe, Y. Non-Alternant Non-Benzenoid Kekulenes: The Birth of a New Kekulene Family. *Chem. Soc. Rev.* **2015**, *44*, 6560–6577.
- (17) Clar, E. The Aromatic Sextet; Wiley: London, 1972; p 74.
- (18) Diederich, F.; Staab, H. A. Benzenoid *versus* Annulenoid Aromaticity: Synthesis and Properties of Kekulene. *Angew. Chem., Int. Ed. Engl.* 1978, 17, 372–374.
- (19) Krieger, C.; Diederich, F.; Schweitzer, D.; Staab, H. A. Molecular Structure and Spectroscopic Properties of Kekulene. *Angew. Chem., Int. Ed. Engl.* **1979**, *18*, 699–701.
- (20) Staab, H. A.; Diederich, F.; Krieger, C.; Schweitzer, D. Molecular Structure and Spectroscopic Properties of Kekulene. *Chem. Ber.* 1983, 116, 3504–3512.
- (21) Pozo, I.; Majzik, Z.; Pavliček, N.; Melle-Franco, M.; Guitián, E.; Peña, D.; Gross, L.; Pérez, D. Revisiting Kekulene: Synthesis and Single-Molecule Imaging. *J. Am. Chem. Soc.* **2019**, *141*, 15488–15493.
- (22) Majewski, M. A.; Hong, Y.; Lis, T.; Gregoliński, J.; Chmielewski, P. J.; Cybińska, J.; Kim, D.; Stępień, M. Octulene: A Hyperbolic Molecular Belt that Binds Chloride Anions. *Angew. Chem., Int. Ed.* **2016**, *55*, 14072–14076.
- (23) Puschnig, P.; Berkebile, S.; Fleming, A. J.; Koller, G.; Emtsev, K.; Seyller, T.; Riley, J. D.; Ambrosch-Draxl, C.; Netzer, F. P.; Ramsey, M. G. Reconstruction of Molecular Orbital Densities from Photoemission Data. *Science* **2009**, *326*, 702–706.
- (24) Puschnig, P.; Reinisch, E. M.; Ules, T.; Koller, G.; Soubatch, S.; Ostler, M.; Romaner, L.; Tautz, F. S.; Ambrosch-Draxl, C.; Ramsey, M. G. Orbital Tomography: Deconvoluting Photoemission Spectra of Organic Molecules. *Phys. Rev. B: Condens. Matter Mater. Phys.* **2011**, 84, 235427.
- (25) Puschnig, P.; Ramsey, M. G. In *Encyclopedia of Interfacial Chemistry: Surface Science and Electrochemistry*; Wandelt, K., Ed.; Elsevier Science: Oxford, 2018; pp 380–391.
- (26) Lüftner, D.; Ules, T.; Reinisch, E. M.; Koller, G.; Soubatch, S.; Tautz, F. S.; Ramsey, M. G.; Puschnig, P. Imaging the Wave Functions of Adsorbed Molecules. *Proc. Natl. Acad. Sci. U. S. A.* **2014**, *111*, 605–610.

- (27) Lüftner, D.; Weiß, S.; Yang, X.; Hurdax, P.; Feyer, V.; Gottwald, A.; Koller, G.; Soubatch, S.; Puschnig, P.; Ramsey, M. G.; Tautz, F. S. Understanding the Photoemission Distribution of Strongly Interacting Two-Dimensional Overlayers. *Phys. Rev. B: Condens. Matter Mater. Phys.* **2017**, *96*, 125402.
- (28) Wießner, M.; Hauschild, D.; Sauer, C.; Feyer, V.; Schöll, A.; Reinert, F. Complete Determination of Molecular Orbitals by Measurement of Phase Symmetry and Electron Density. *Nat. Commun.* **2014**, *5*, 4156.
- (29) Weiß, S.; Lüftner, D.; Ules, T.; Reinisch, E. M.; Kaser, H.; Gottwald, A.; Richter, M.; Soubatch, S.; Koller, G.; Ramsey, M. G.; Tautz, F. S.; Puschnig, P. Exploring Three-Dimensional Orbital Imaging with Energy-Dependent Photoemission Tomography. *Nat. Commun.* **2015**, *6*, 8287.
- (30) Yang, X.; Egger, L.; Hurdax, P.; Kaser, H.; Lüftner, D.; Bocquet, F. C.; Koller, G.; Gottwald, A.; Tegeder, P.; Richter, M.; Ramsey, M. G.; Puschnig, P.; Soubatch, S.; Tautz, F. S. Identifying Surface Reaction Intermediates with Photoemission Tomography. *Nat. Commun.* **2019**, *10*, 3189.
- (31) Graus, M.; Grimm, M.; Metzger, C.; Dauth, M.; Tusche, C.; Kirschner, J.; Kümmel, S.; Schöll, A.; Reinert, F. Electron-Vibration Coupling in Molecular Materials: Assignment of Vibronic Modes from Photoelectron Momentum Mapping. *Phys. Rev. Lett.* **2016**, *116*, 1–5.
- (32) Kliuiev, P.; Zamborlini, G.; Jugovac, M.; Gurdal, Y.; Arx, K. V.; Waltar, K.; Schnidrig, S.; Alberto, R.; Iannuzzi, M.; Feyer, V.; Hengsberger, M.; Osterwalder, J.; Castiglioni, L. Combined Orbital Tomography Study of Multi-Configurational Molecular Adsorbate Systems. *Nat. Commun.* **2019**, *10*, 5255.
- (33) Kruszewski, J.; Krygowski, T. M. Definition of Aromaticity Basing on the Harmonic Oscillator Model. *Tetrahedron Lett.* **1972**, *13*, 3839–3842.
- (34) Krygowski, T. M. Crystallographic Studies of Inter- and Intramolecular Interactions Reflected in Aromatic Character of π -Electron Systems. *J. Chem. Inf. Model.* **1993**, 33, 70–78.
- (35) Krygowski, T. M.; Cyrański, M. Separation of the Energetic and Geometric Contributions to the Aromaticity of π -Electron Carbocyclics. *Tetrahedron* **1996**, *52*, 1713–1722.
- (36) Krygowski, T. M.; Cyrański, M. Separation of the Energetic and Geometric Contributions to the Aromaticity. Part IV. A General Model for the π -Electron Systems. *Tetrahedron* **1996**, *52*, 10255–10264
- (37) Setiawan, D.; Kraka, E.; Cremer, D. Hidden Bond Anomalies: The Peculiar Case of the Fluorinated Amine Chalcogenides. *J. Phys. Chem. A* **2015**, *119*, 9541–9556.
- (38) Firme, C. L.; Galembeck, S. E.; Antunes, O. A.; Esteves, P. M. Density, Degeneracy, Delocalization-Based Index of Aromaticity (D₃BIA). *J. Braz. Chem. Soc.* **2007**, *18*, 1397–1404.
- (39) Araújo, D. M.; da Costa, T. F.; Firme, C. L. Validation of the Recently Developed Aromaticity Index D3BIA for Benzenoid Systems. Case Study: Acenes. *J. Mol. Model.* **2015**, *21*, 248.
- (40) Stępień, M. An Aromatic Riddle: Decoupling Annulene Conjugation in Coronoid Macrocycles. *Chem.* **2018**, *4*, 1481–1483.
- (41) Aihara, J.-i. Validity and Limitations of the Annulene-Within-An-Annulene (AWA) Model for Macrocyclic π -Systems. *RSC Adv.* **2014**. 4, 7256–7265.
- (42) Casademont-Reig, I.; Ramos-Cordoba, E.; Torrent-Sucarrat, M.; Matito, E. How Do the Hückel and Baird Rules Fade Away in Annulenes? *Molecules* **2020**, *25*, 711.
- (43) Hückel, E. Die freien Radikale der organischen Chemie. Z. Physik 1933, 83, 632–668.
- (44) Coulson, C. A. The Electronic Structure of Some Polyenes and Aromatic Molecules VII. Bonds of Fractional Order by the Molecular Orbital Method. *Proc. R. Soc. London* **1939**, *169*, 413–428.
- (45) Tian, H.; Shi, J.; Dong, S.; Yan, D.; Wang, L.; Geng, Y.; Wang, F. Novel Highly Stable Semiconductors Based on Phenanthrene for Organic Field-Effect Transistors. *Chem. Commun.* **2006**, 3498–3500.

- (46) Gottwald, A.; Kaser, H.; Kolbe, M. The U125 Insertion Device Beamline at the Metrology Light Source. *J. Synchrotron Radiat.* **2019**, 26, 535–542.
- (47) Broekman, L.; Tadich, A.; Huwald, E.; Riley, J.; Leckey, R.; Seyller, T.; Emtsev, K.; Ley, L. First Results From a Second Generation Toroidal Electron Spectrometer. *J. Electron Spectrosc. Relat. Phenom.* **2005**, *144*–*147*, 1001–1004.
- (48) Haags, A.; Reichmann, A.; Fan, Q.; Egger, L.; Kirschner, H.; Naumann, T.; Werner, S.; Vollgraff, T.; Sundermeyer, J.; Eschmann, L.; Yang, X.; Brandstetter, D.; Bocquet, F. C.; Koller, G.; Gottwald, A.; Richter, M.; Ramsey, M. G.; Rohlfing, M.; Puschnig, P.; Gottfried, J. M.; et al. *Kekulene: On-Surface Synthesis, Orbital Structure, and Aromatic Stabilization*, 2020, 12771254, ChemRxiv. https://doi.org/DOI: 10.26434/chemrxiv.12771254.v1, Accessed: August 07, 2020.
- (49) Haags, A.; Reichmann, A.; Fan, Q.; Egger, L.; Kirschner, H.; Naumann, T.; Werner, S.; Vollgraff, T.; Sundermeyer, J.; Eschmann, L.; Yang, X.; Brandstetter, D.; Bocquet, F. C.; Koller, G.; Gottwald, A.; Richter, M.; Ramsey, M. G.; Rohlfing, M.; Puschnig, P.; Gottfried, J. M.; Soubatch, S.; Tautz, F. S. Data used in: "Kekulene: On-Surface Synthesis, Orbital Structure, and Aromatic Stabilization", 2020, Jülich DATA, https://doi.org/10.26165/JUELICH-DATA/UVHBRU.